Distance and Orientation Dependence of Excitation Transfer Rates in Conjugated Systems: Beyond the Förster Theory

Kim F. Wong,[§] Biman Bagchi,*[,†] and Peter J. Rossky*

Institute for Theoretical Chemistry, Department of Chemistry and Biochemistry, University of Texas at Austin, Austin, Texas 78712-1167

Received: December 5, 2003

The distance (R_{DA}) and orientation dependence of the rate for electronic excitation transfer (EET) from a segment of polyfluorene (PF_6) to tetraphenylporphyrin (TPP) is studied using semiempirical quantum chemical methods. The fundamental issue concerns the applicability of the traditional Förster theory, which uses a point-dipole approximation, in describing the transfer rate in such systems involving large chromophores that may approach each other closely. In our theoretical calculation of the resonance-Coulomb rate, explicit account is taken of the extended transition dipole moment densities that are spread along the donor and acceptor molecules. Although we recover the Förster rate at large separations, the present study reveals several results not anticipated in the conventional theory: (a) The actual rate shows a much weaker short-range distance dependence (closer to R_{DA}^{-2} than to the Förster R_{DA}^{-6} value). The Förster expression overestimates the energy transfer rate by more than 2 orders of magnitude at short separation ($R_{DA} < 1$ nm). (b) The distance at which the Förster rate is recovered is observed to be rather large (∼10 nm). Thus, the Förster expression seems to be inappropriate for condensed-phase systems where donors and acceptors can be closely packed, as, for example, in thin films. (c) Significant excitation transfer can occur via states that are optically dark (that is, carry very small oscillator strength). Förster theory excludes these potentially important pathways. (d) Irrespective of the interchromophore separation, the calculated orientation dependence of the resonance-Coulomb rates generally follows the Förster expression, with dependence on the cosine of the angle between the donor and acceptor transition dipole moment vectors. At close distances, however, the orientation dependence can make the rates differ by a factor of ∼2.

1. Introduction

The fluorescence resonance energy transfer (FRET) phenomenon has provided physicists, chemists, and biologists with a very powerful and versatile tool for studying the structure and dynamics of large molecules in the condensed phases. Because the scale for energy transfer is strongly dependent on the distance between the donor and the acceptor, FRET has been used to study the folding of proteins and DNA, as well as the conformational dynamics of other polymers. In many important photophysical and photochemical processes, the excitation energy of an excited state can migrate, by the same resonance transfer process, over a long distance before the energy is emitted as light (as in many conjugated polymers) or used up in chemical reactions, as in the photosynthetic reaction center. The dynamics of this process can often be studied optically. Because this transfer process is central to the efficient conversion of solar energy to chemically storable forms in plants and bacteria, the mechanism of this long-range energy transfer has been a subject of much attention in the past few decades.[1−15] Light-harvesting antenna complexes, for example, can collect and channel solar energy to the reaction center with 95% overall efficiency. It is believed that excitation transfer in conjugated polymers is similarly facile and that this process ultimately influences the optoelectronic function of devices fabricated from these organic semiconductors.[16] The study of electronic excitation energy transfer (EET) mechanisms has taken an additional importance because of the discovery that, in a thin film environment, a conjugated polymer can consist of long rodlike stiff segments that are broken by quenched chemical defects.[17−19] Excitation transfer in such a polymeric system may be quite different from that in a random-coil polymer, which has been often considered.[20,21] The interchain migration rate ultimately will be dependent on the relative internal geometries between the donor and acceptor chromophores. An understanding of the spatial and orientation dependence of the excitation transfer is therefore one key to optimizing the performance of molecular-based devices involving electronic excitation transfer.

Despite the great interest in this process and the routine use of the Förster mechanism[22−39] to explain the optical properties of conjugated polymers, there have been surprisingly few microscopic calculations of the transfer rate.[40,41] Such a calculation should start directly from the Fermi Golden rule rate expression and evaluate the Coulomb matrix element within the donor−acceptor basis set.[42−49] Although the Förster theory[37,38] conveniently relates the transfer rate to experimentally measurable donor fluorescence and acceptor absorption spectra via the simple and elegant expression

$$k_{DA}^{\text{Förster}}(R_{DA}) = k_D^{rad}\left(\frac{R_F}{R_{DA}}\right)^6 \quad (1)$$

the point-dipole approximation used in the formulation is expected to be inadequate at short distances, particularly when the electrostatics of the donor and acceptor systems themselves are extended, as in the case of conjugated polymers.[50,51] In the

* Author to whom correspondence should be addressed.
§ Current address: Department of Chemistry, 152 Davey Laboratory, Pennsylvania State University, University Park, PA 16802.
† Permanent address: Solid State and Structural Chemistry Unit, Indian Institute of Science, Bangalore, 560012, India.

10.1021/jp037724s CCC: $27.50
Published on Web 06/15/2004

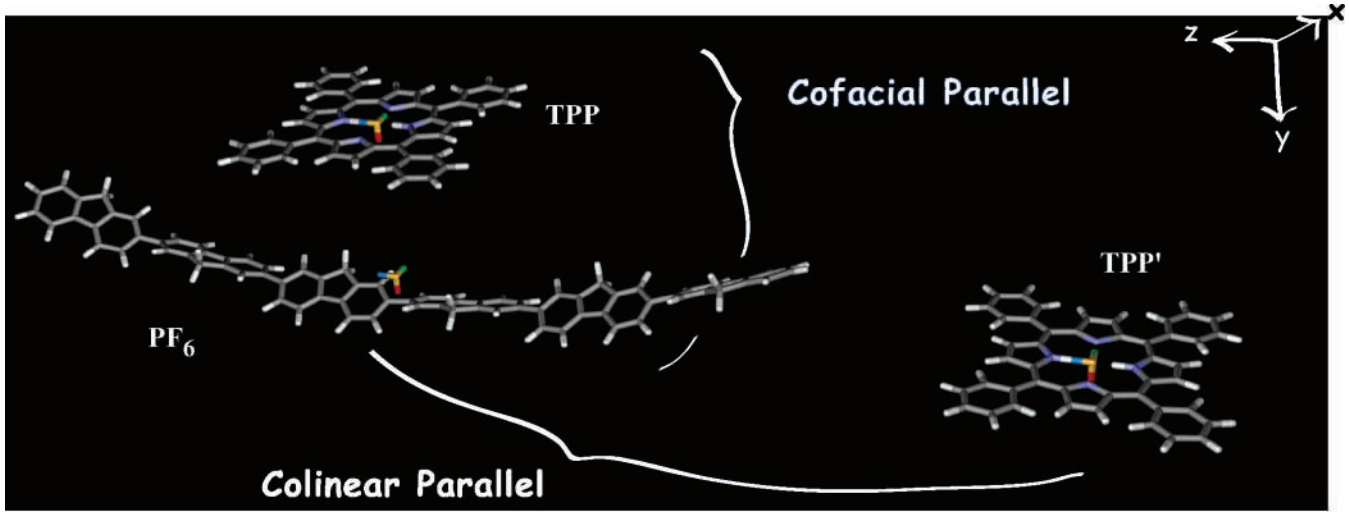

Figure 1. Schematic representation of the donor chromophore polyfluorene (PF_6) and the acceptor chromophore tetraphenylporphyrin (TPP) in an arrangement where the transition dipole moments are aligned (1) parallel to each other and (2) orthogonal to the donor−acceptor (DA) intermolecular axis (cofacial parallel) and parallel to the DA intermolecular axis (collinear parallel). The related cofacial orthogonal and collinear orthogonal orientations are similar in arrangement, except that the TPP acceptor has been rotated 90° about the *y*-axis such that the transition dipole moment vectors are orthogonal to each other. The red green blue (RGB) axes define the reference frame of each molecule, whereas the *B*-axis (*z*-axis) shows the direction of the transition dipole moment vector.

aforementioned rate expression, k_D^{rad} denotes the donor radiative decay rate and R_F represents the Förster radius, which can be expressed as an overlap integral between the donor emission $I_D(\omega)$ and acceptor absorption $\alpha_A(\omega)$ spectra:

$$R_F^6 \propto \kappa_{DA}^2 \int_0^\infty \frac{d\omega}{\omega^4} I_D(\omega)\alpha_A(\omega) \quad (2)$$

The orientation factor κ_{DA}^2, which takes into account the effect of the relative orientation of the two transition dipole moment vectors (see Figure 1), is given by

$$\kappa_{DA}^2 = (\sin\theta_D \sin\theta_A \cos\Phi_{ARD} - 2\cos\theta_D \cos\theta_A)^2 \quad (3)$$

where θ_D and θ_A are the angles that the donor and acceptor transition dipole moments, respectively, make with the intermolecular separation vector R_{DA} and Φ_{ARD} is the dihedral angle defined by the corresponding three vectors. A quick inspection of the orientation factor shows that the κ_{DA}^2 value can range from 0 to 4. It is common to assume a random orientational average value of $^2/_3$, because this parameter is not easily extracted from most experiments.

The explicit connection of the Förster rate to optically bright states highlights another limitation of the approach. Fleming and co-workers have investigated the appropriateness of Förster theory in the context of energy transfer dynamics in aggregated molecular assemblies.[42−45] These authors not only presented a general formalism for calculating the energy transfer rate in multiple donor−acceptor systems, but also illustrated the two aforementioned limitations of the Förster expression. Their results show that, at short distances, the rate can be considerably different from the prediction of the Förster rate, which is due to the transfer to optically dark acceptor states.[43] Recently, Beljonne et al. compared the relative rates of interchain to intrachain EET in acceptor-capped conjugated polymers using a multicentric distributed monopole method.[40] Their calculations show that intramolecular energy transport along segments of a polymer is intrinsically slow, compared to intermolecular transfer between polymer chains. Although interchain excitation transfer occurs within a few tens of picoseconds, intrachain transfer proceeds on a nanosecond time scale (a slow rate compared to typical excited-state depopulation rates of conjugated polymers). Their results also indicate that their multicentric formulation of EET is less sensitive to donor−acceptor orientation then is Förster theory. Thus, although one clearly knows that the Förster expression is inadequate at short separation between the donor and the acceptor, not much seems to be known about the quantitative aspects of this dependence.

In the present study, we investigate the distance and orientation dependence of EET between a six-unit oligomer of polyfluorene (PF_6) and tetraphenylporphyrin (TPP); the chemical structure and representative orientations of the two are given in Figure 1. In this system, one expects very efficient energy transfer from the blue-emitting conjugated polymer (at ∼420 nm) to the red-emitting TPP guest molecules (at ∼620 nm).[52] Such systems are of interest, because related host−guest systems comprised of polymer/polymer and polymer/dye blends are currently being utilized to achieve color tunability and saturated color emission[53,54] in displays, as well as to reduce self-absorption loss in laser applications.[55−57] Cerullo et al. recently observed ultrafast EET on the picosecond time scale from poly(9,9-dioctylfluorene) (PFO) to TPP in thin films using femtosecond pump−probe spectroscopy.[52] When fitting their results to the Förster expression, they obtained a value of 4.2 nm for the Förster radius. Considering that typical radiative lifetime for conjugated polymers is on the order of a nanosecond and that the Förster rate dissipates as R_{DA}^{-6} with increasing donor−acceptor (DA) separation, the excitation must be transferring at a distance of ∼1 nm or less (see eq 1). This is the regime where one expects the Förster treatment to be most limited. An approach that goes beyond the point-dipole simplification is necessary for treating molecular assemblies with similar length scales; we present such an approach in this paper. Our main objectives for studying this particular system is that it provides us with a well-defined, experimentally accessible and computationally tractable system that can be used to answer fundamental questions about excitation transfer, particularly, the distance and orientation dependence of the rate in conjugated polymeric systems.

The computational approach used in this study is based on a classic semiempirical Pariser−Parr−Pople (PPP) Hamiltonian,[58−60]

coupled with single configuration interaction (SCI).[61] The PPP electronic structure method has proved to be quite adequate in reproducing the electronic transition energies of related PPV class of conjugated polymers and similar conjugated ring heterocycles.[17,62−65] From the PPP/SCI wave functions, electronic transition energies, and transition dipole moments (at optimized geometries of PF_6 and TPP), we compute the full resonance-Coulomb coupling matrix element as well as the point-dipole approximation to the coupling. Combined with molecular visualization, this method allows us to explore the geometrical aspect of excitation transfer and to delineate the limitations of the Förster theory. We find the following main results. For a given orientation, the transfer rate between a rigid segment of PF_6 and TPP varies rather slowly ($\sim R_{DA}^{-2}$) at short distances. To obtain the familiar R_{DA}^{-6} form quantitatively, one must reach an R_{DA} value of ~10 nm. In qualitative agreement with time-resolved experimental results,[52] the resonance-Coulomb rate at short distances is on the order of 10^{12} s^{-1}. At the same separations, the Förster expression would predict a rate close to 10^{15} s^{-1}. We find that a significant amount of energy transfer can occur to optically dark acceptor states, that is, to states that have very small oscillator strengths. These processes are not included in the conventional Förster formulation where the rate is proportional to the spectral overlap of the donor emission and acceptor absorption. For a given DA separation, both the Förster and resonance-Coulomb rates effectively follow a cosine function of the angle between the DA transition dipole moment vectors, although the absolute rates are dependent on the theory used. However, for fixed parallel orientation of transition dipole vectors at close DA separation, the resonance-Coulomb rate can vary by a factor of ~2, depending on the degree of rotation about the acceptor transition dipole axis. Even at the Förster radius, such orientation dependence can provide resonance-Coulomb rates that vary by 30%. The corresponding Förster rates lack this orientation dependence. In the orthogonal arrangement of transition dipole moment vectors at close DA separation, the resonance-Coulomb rates can differ from Förster theory by 3 orders of magnitude; however, the rates in this arrangement are on a time scale of nanoseconds, so these rates are not expected to be of practical interest.

The organization of the remainder of the paper is as follows. To clarify the approximations inherent in Förster theory, we provide in the next section a brief derivation of the Förster rate equation, starting from the Fermi Golden rule expression. An alternative approach, which bypasses these approximations, is also presented for calculating EET rates within a microscopic framework based on quantum chemical methods. We then describe the details of our numerical implementation. The Results and Discussion section delineates the Förster and non-Förster regimes of EET by comparing the distance and orientation dependence of the transfer rates from the two methods. Last, we assess the impact of the present results on the interpretation of experimental studies of excitation transfer and conclude with prospects for further study.

2. Theoretical Formulation

The electronic excitation transfer process can be broadly characterized into two categories: coherent and incoherent.[41,66] The coherent case corresponds to the strong electronic coupling limit where the time scale of EET is much faster than that of vibrational relaxation. An initial local excitation of the donor, thus, rapidly delocalizes spatially across both the donor and acceptor chromophores. The system can then be represented simply as a two-level model comprised of linear combinations of localized excitation on the donor and localized excitation on the acceptor. Emission from excimers and exciplexes are radiative signatures of the aftermath of EET in the strong coupling limit. At relatively high temperatures and in relatively disordered systems such as thin films of conjugated polymers, it is believed that the coupling is weak and, thus, the relevant excitation migration can be assumed to be incoherent. In this limit, fast nuclear relaxation localizes the initial excitation prior to EET; subsequent relaxation and localization of the excitation on the acceptor effectively makes the entire process irreversible. One then can describe the electronic excitation migration as a random walk between pairs of donor and acceptor molecules.[20] The presence of excimers and aggregates in polymer thin films have been correlated with the reduction in photoluminescence quantum yield (possibly due to EET to these low-energy traps). However, the present study of EET will concentrate only on those elements associated with weak coupling. The analysis developed here, nonetheless, would also be applicable to excimers. However, the detrimental role of such photophysical traps is important and is an appropriate subject for future study.

Mediated by the Coulombic interactions between the donor and acceptor electronic states, electronic excitation transfer involves the simultaneous de-excitation of the donor and excitation of the acceptor chromophores. The initial state is composed of a direct product of the donor in the excited state with the acceptor in the ground state, $|\Psi_{D^*}^M \Psi_{A0}^N\rangle = |\psi_D^* \chi_{D^*}^M \psi_A^0 \chi_{A0}^N\rangle$, where $\chi_{D^*}^M$ is the Mth vibrational state of the excited electronic state of the donor ψ_D^* and χ_{A0}^N is the Nth vibrational state of the acceptor in the ground electronic state ψ_A^0. The final state describes the composite system with the donor in the ground state and the acceptor in the excited state, $|\Psi_{D0}^S \Psi_{A^*}^T\rangle$. Within first-order time-dependent perturbation theory, the thermal average transition rate is given by the Fermi Golden rule,

$$k_{DA} = \frac{2\pi}{\hbar} \sum_{\{M,N\}} \sum_{\{S,T\}} f(E_{D^*}^M)\, f(E_{A0}^N) \left|\langle \Psi_D^M \Psi_{A0}^N \left| V_{DA}^{Coul} \right| \Psi_{D0}^S \Psi_{A^*}^T \rangle\right|^2 \times \delta(E_{D^*}^M + E_{A0}^N - E_{A^*}^T - E_{D0}^S) \quad (4)$$

where the sum over the sets of quantum states of nuclear modes on the initial electronic surface $\{M, N\}$ averages over the quantum distribution of initial conditions with weights $f(E_{D^*}^M)$ and $f(E_{A0}^N)$, and the sum over $\{S, T\}$ times the delta function includes the final nuclear states that conserve the total energy. In the Condon approximation, the matrix element of the Coulomb operator reduces to an electronic coupling weighted by Franck−Condon overlaps between the initial and final vibrational states:

$$\langle \Psi_{D^*}^M \Psi_{A0}^N | V_{DA}^{Coul} | \Psi_{D0}^S \Psi_{A^*}^T \rangle = \langle \psi_D^* \psi_A^0 | V_{DA}^{Coul} | \psi_D^0 \psi_A^* \rangle \langle \chi_{D^*}^M | \chi_{D0}^S \rangle \langle \chi_{A0}^N | \chi_{A^*}^T \rangle \quad (5)$$

V_{DA}^{Coul} denotes the Coulomb potential,

$$V_{DA}^{Coul} = \frac{1}{2} \sum_{j,k} \frac{e^2}{|\boldsymbol{R}_{DA} + \boldsymbol{r}_D(j) - \boldsymbol{r}_A(k)|} \quad (6)$$

where $\boldsymbol{R}_{DA}$ represents the distance between the centers of mass of the donor and acceptor and $\boldsymbol{r}_D(j)$ and $\boldsymbol{r}_A(k)$ respectively denote the coordinates of the jth electron of the donor and the kth electron of the acceptor. At short donor−acceptor separation where direct overlap between orbitals of the donor and the

acceptor occurs, the exchange integral in the electronic coupling dominates the interaction and the transfer proceeds via the so-called Dexter mechanism.[67] The Dexter rate decreases exponentially with distance as $\exp(-R_{DA}/\lambda_D)$, where λ_D is the Dexter radius (typically <5 Å). For DA separations beyond van der Waals contact, the Coulomb integral dominates and the transfer proceeds via the long-range resonance-Coulombic interaction of the DA transition dipole densities.[68,69] Although the Dexter mechanism can be operative for some molecular assemblies, it is unlikely to be the dominant mechanism in the case of the conjugated polymers, where the distance of closest approach between the DA pairs is hindered by steric interactions. The main source of the steric hindrance are the flexible side groups, which are normally functionalized onto the backbone to increase solubility. Thus, the resonance-Coulomb mechanism is believed to be the main cause of electronic excitation transfer in conjugated polymers. If one expands eq 6 in a multipole expansion in powers of $|\boldsymbol{r}_D(j) - \boldsymbol{r}_A(k)|/|\boldsymbol{R}_{DA}|$ and keep terms only up to second order, one can express the electronic coupling in terms of transition dipole moments:

$$\langle \psi_D^* \psi_A^0 | V_{DA}^{Coul} | \psi_D^0 \psi_A^* \rangle \approx \frac{\boldsymbol{d}_D \cdot \boldsymbol{d}_A}{|\boldsymbol{R}_{DA}|^3} - 3\frac{(\boldsymbol{R}_{DA}\cdot\boldsymbol{d}_D)(\boldsymbol{R}_{DA}\cdot\boldsymbol{d}_A)}{|\boldsymbol{R}_{DA}|^5} \quad (7)$$

$$= \kappa_{DA}\frac{|\boldsymbol{d}_D||\boldsymbol{d}_A|}{|\boldsymbol{R}_{DA}|^3}$$

where the orientational factor is defined as $\kappa_{DA} = \boldsymbol{n}_D\cdot\boldsymbol{n}_A - 3(\boldsymbol{e}_{DA}\cdot\boldsymbol{n}_D)(\boldsymbol{e}_{DA}\cdot\boldsymbol{n}_A)$, where $\boldsymbol{n}_D$ and $\boldsymbol{e}_{DA}$ are unit vectors pointing in the directions of the transition dipole moment $\boldsymbol{d}_D$ and donor−acceptor distance vector $\boldsymbol{R}_{DA}$, respectively. To obtain the Förster expression for the rate in terms of the $S_1 \rightarrow S_0$ donor emission spectrum and the $S_0 \rightarrow S_1$ acceptor absorption spectrum, one decouples the transition dipole moment of the donor from that of the acceptor and rewrites the delta function in the rate as

$$\delta(E_{D^*}^M + E_{A^0}^N - E_{A^*}^T - E_{D^0}^S) = \int_{-\infty}^{\infty} dE\,\delta(E_{D^*}^M - E_{D^0}^S - \hbar\omega)\delta(E_{A^0}^N - E_{A^*}^T + \hbar\omega) \quad (8)$$

where E is the excitation energy involved in the transfer ($E = \hbar\omega$). The donor transition dipole moment then is related to the donor fluorescence spectrum by

$$I_D(\omega) = \frac{4\eta^3\omega^3}{3\hbar c^3}|\boldsymbol{d}_D|^2\sum_{\{M\}}\sum_{\{S\}} f(E_{D^*}^M)\left|\langle\chi_{D^*}^M|\chi_{D^0}^S\rangle\right|^2 \times \delta(E_{D^*}^M - E_{D^0}^S - \hbar\omega) \quad (9)$$

and the acceptor transition dipole moment is related to the acceptor absorption coefficient by

$$\alpha_A(\omega) = \frac{4\pi^2\eta\omega}{3c}|\boldsymbol{d}_A|^2\sum_{\{N\}}\sum_{\{T\}} f(E_{A^0}^N)\left|\langle\chi_{A^0}^N|\chi_{A^*}^T\rangle\right|^2 \times \delta(E_{A^0}^N - E_{A^*}^T + \hbar\omega) \quad (10)$$

where the inclusion of the index of refraction η accounts for the effect of the medium on the speed of light (c). The final rate expression

$$k_{DA}^{Förster} = \frac{9\hbar c^4\kappa_{DA}^2}{8\pi\eta|\boldsymbol{R}_{DA}|^6}\int_0^\infty \frac{d\omega}{\omega^4} I_D(\omega)\alpha_A(\omega) \quad (11)$$

is dependent on the fluorescence and absorption characteristics of the donor and acceptor, respectively, and the rate decreases as the sixth power with increasing donor−acceptor separation. It is common to express the Förster rate in the simpler and elegant form of eq 1, where the Förster radius R_F is defined as the critical separation for which the excitation transfer rate is equal to the radiative decay rate of the isolated donor chromophore. Note that while fitting the Förster expression to experimental EET rates, one must determine k_D^{rad} and R_F independently. The computation of R_F also entails performing an unrestricted averaging over the ensemble of orientations between the donor and acceptor chromophores (see eq 2).[70−72]

In terms of the fluorescence $F_D(\omega)$ and the absorption $A_A(\omega)$ line shapes, with each normalized to a unit area on an energy scale, the EET rate takes an alternative, more general, form that does not invoke an expansion of the Coulomb operator for large separation, namely

$$k_{DA} = \frac{2\pi}{\hbar}|\langle V_{DA}^{Coul}\rangle|^2\int_0^\infty d\omega F_D(\omega)A_A(\omega) \quad (12)$$

where $J \equiv \int_0^\infty d\omega F_D(\omega)A_A(\omega)$ is the spectral overlap integral and $\langle V_{DA}^{Coul}\rangle$ denotes the matrix element of the Coulomb potential between the initial and final electronic states. The Franck−Condon factors and energy conservation condition is contained within this spectral overlap integral. In the point-dipole approximation, eq 12 reduces to the Förster expression.

Notably, at this juncture, the expression in eq 12 does not explicitly assume that the donor and acceptor states involved are bright states. The Coulomb coupling between dark states, or between bright and dark states, can also be obtained from $\langle V_{DA}^{Coul}\rangle$. However, the Franck−Condon factors for vibronic states satisfying energy conservation are not provided by the line shape overlap in the equations, because the dark states do not, of course, contribute there. In the following calculations, we treat both the bright and dark states in terms of the same generic line shape and overlap (see Section 2.1); that treatment simply creates the same dependence on the DA energy gap for all state pairs (see eq 14, below).

As discussed by others previously, this multipole expansion in powers of $|\boldsymbol{r}_D(j) - \boldsymbol{r}_A(k)|/|\boldsymbol{R}_{DA}|$ should become unreasonable when the distance $|\boldsymbol{r}_D(j) - \boldsymbol{r}_A(k)|$ becomes comparable to $|\boldsymbol{R}_{DA}|$. This happens at relatively large values of $|\boldsymbol{R}_{DA}|$, in the case of spatially extended systems, such as conjugated polymers. For such systems and distances, one must evaluate the full resonance-Coulomb matrix element directly, using quantum chemical methods.

3. Computational Details

We have considered excitation transfer from an oligomer of fluorene with degree of polymerization of 6 to a TPP molecule, with both the donor and the acceptor held fixed at a set of distances and orientations. The optimized first singlet excited-state geometries of the donor PF_6 was obtained within the semiempirical AM1[73] model with complete active space configuration interaction (CI); the active space was increased systematically until convergence of the energy occurred. The optimized ground-state structure of TPP was obtained with an AM1 single determinant treatment. From the optimized geometries, we form the matrix element of the Coulomb operator between wave functions described within the simpler PPP Hamiltonian.[58−60] The excited state consists of a linear combination of single excitation determinants, whereas the SCF determinant describes the ground state. One-center repulsion

and core parameters, used in our PPP implementation, were derived from the spectroscopic data of Hinze and Jaffe.[63,74] The two-electron repulsion matrix elements were obtained from the Mataga−Nishimoto equation,[75] whereas the resonance integrals follow directly from the Linderberg equation,[76] using Slater 2p atomic orbitals. Electronic transition energies to excited states and the corresponding oscillator strengths were obtained from configuration interaction with all possible single excitations (SCI).[61] Similar procedures applied to related conjugated systems, including ring heterocycles, were successful in reproducing experimental spectra.[17,62−65]

One can then readily evaluate the matrix element of the Coulomb potential between electronic states described within the PPP method.[58−60] The electronic coupling takes the form

$$\langle \psi_D^* \psi_A^0 | V_{DA}^{Coul} | \psi_D^0 \psi_A^* \rangle = \sum_{\substack{ar \\ \in\{D\}\in\{A\}}} \sum_{a'r'} C_a^r C_{a'}^{r'} \left[2 \sum_{\mu\nu} c_\mu^r c_\mu^a c_\nu^{a'} c_\nu^{r'} \gamma_{\mu\nu} \right] \quad (13)$$

where C_a^r and $C_{a'}^{r'}$ are, respectively, the SCI expansion coefficients describing the donor and acceptor excited states, c_μ^r is the μth expansion coefficient of molecular orbital r, and $\gamma_{\mu\nu}$ is the two-electron repulsion matrix element; the derivation is provided in the Appendix. We note that the SCI and the molecular orbital coefficients that enter into the expression above are obtained from separate calculations for the donor and acceptor molecules. Our calculation of the EET transfer rate proceeds directly from eq 12. In addition to the matrix element, one also needs the spectral overlap integral. Because we do not explicitly treat nuclear motion here (the donor and acceptor geometries are held static), we only have delta function spectra from the singlet excitation energy calculations. The effect of the Franck−Condon factors within the spectral overlaps is to broaden the distribution of transition energies. To mimic this homogeneous broadening, we convolute each "stick" spectra with a Gaussian of width 30 nm centered at each transition energy; this value is comparable to widths used in earlier spectral fittings.[17,50,77] Generally, of course, the widths of the donor and acceptor spectra are particular to the chromophore and environment. However, this rough scheme is sufficient for our current comparative study of the Förster expression and the full rate; the choice of the width parameter affects the absolute radial values but not the relative radial values of the transfer rate (see eqs 15 and 16). The overlap between two Gaussian spectra of equal width σ whose centers are displaced by the amount Δ_{DA} is given by

$$J \approx \frac{\sqrt{\pi}}{2\sigma} \exp\left(-\frac{\Delta_{DA}^2}{4\sigma^2} \right) \quad (14)$$

With all terms thus explicitly defined, the final expressions for the EET rate, within the PPP formalism and within the Förster approximation, are

$$k_{DA} = \frac{2\pi}{\hbar} \left| \sum_{\substack{ar \\ \in\{D\}\in\{A\}}} \sum_{a'r'} C_a^r C_{a'}^{r'} \left[2 \sum_{\mu\nu} c_\mu^r c_\mu^a c_\nu^{a'} c_\nu^{r'} \gamma_{\mu\nu} \right] \right|^2 \frac{\sqrt{\pi}}{2\sigma} \times \exp[-\Delta_{DA}^2/4\sigma^2] \quad (15)$$

$$k_{DA}^{Förster} = \frac{2\pi}{\hbar} \left| \frac{\boldsymbol{d}_D \cdot \boldsymbol{d}_A}{|\boldsymbol{R}_{DA}|^3} - 3\frac{(\boldsymbol{R}_{DA} \cdot \boldsymbol{d}_D)(\boldsymbol{R}_{DA} \cdot \boldsymbol{d}_A)}{|\boldsymbol{R}_{DA}|^5} \right|^2 \frac{\sqrt{\pi}}{2\sigma} \exp\left(-\frac{\Delta_{DA}^2}{4\sigma^2} \right) \quad (16)$$

TABLE 1: Donor and Acceptor Excitation Energy (E) and Oscillator Strength (f)[a]

donor			acceptor		
E (eV)	E (nm)	f	E (eV)	E (nm)	f
3.464	357.897	4.34	1.837	675.113	0.26
3.736	331.866	0.18	1.983	625.087	0.06
3.973	312.104	0.82	2.893	428.637	2.00
4.206	294.790	0.08	2.964	418.330	1.44
4.453	278.446	0.36	3.182	389.649	0.70
4.899	253.075	0.14	3.378	367.078	0.38
			3.663	338.514	0.26
			3.671	337.769	0.06
			3.793	326.848	0.10
			4.075	304.289	0.22

[a] The experimental absorption spectrum of the PFO donor peaks at 385 nm, whereas the absorption spectrum of the TPP acceptor peaks at 418 nm.

The standard form of the Förster rate equation (eq 11) is written in terms of experimental fluorescence and absorption spectra, with an orientation factor reflecting the ensemble average of relative orientations between the donors and acceptors. The transition dipole moment vectors are embedded within the fluorescence (eq 9) and absorption (eq 10) spectra and are experimentally inaccessible. We have the actual transition dipole moment vectors within our microscopic formulation of EET; therefore, we directly compute the point-dipole approximation to the resonance-Coulomb coupling. For a specific donor−acceptor orientation, one would need to sum over the rates between all pairs of DA excitation transition energies. The macroscopic rate also entails averaging over an ensemble of microscopic donor−acceptor orientations representative of the bulk system.

4. Results and Discussion

The spatial extent, intermolecular separation, and relative orientations of transition dipole densities on the donor and acceptor chromophores can be viewed as ultimately determining the rate of electronic excitation transfer. While it is routine to analyze experimental measurements according to Förster theory, as noted previously, such a point-dipole approximation to the rate is expected to be invalid when the transition dipole densities are distributed on a length scale similar to the DA separation. Considering that the first singlet exciton state in conjugated polymers is delocalized over a few monomer units spanning ~20 Å or more,[17,50,51,78,79] excitation transfer in this class of materials is expected to include the non-Förster regime. The limitations of the point-dipole formulation are delineated in this section by comparing the calculated distance and orientation dependence of the Förster rate to the full resonance-Coulomb rate calculated from identical wave functions.

Because electronic transitions are fundamental to the theory, we begin by presenting the values obtained here for singlet excitation energies and corresponding oscillator strengths for the donor PF_6 and acceptor TPP molecules (Table 1). As the geometry of the donor molecule corresponds to the optimized geometry in the first excited state, the donor transition energies represent fluorescence, whereas the transition energies for the optimized ground-state acceptor represent absorption. The key motivation in deciding to optimize PF_6 in the lowest excited state rather than in other higher excited states is that it is the dominant optically active mode (Table 1; 358 nm) and that the nuclear relaxation of the donor is expected to precede energy transfer to an acceptor. Thus, it seems justified to assume that EET occurs from the relaxed lowest excited state of the donor

TABLE 2: Coupling Strength as a Function of Intermolecular Distance (R_{DA}) between the Donor and Acceptor Centers of Mass for the Cofacial Parallel Orientation (See Figure 1) of the Donor d_D (358 nm) and Acceptor d_A (367 nm) Transition Dipole Moments

R_{DA} (Å)	$(V_{DA}^{Coul})^2$ (10^{-43} J^2)	$(d_D d_A/R_{DA}^3)^2$ (10^{-43} J^2)	k_{DA}	$k_{DA}^{Förster}$
5	57.18	64 029	1.0 ps^{-1}	980.0 ps^{-1}
10	19.15	1000	320.5 ns^{-1}	15.3 ps^{-1}
20	2.672	15.631	42.7 ns^{-1}	239.3 ns^{-1}
40	0.133	0.244	2.1 ns^{-1}	3.7 ns^{-1}
100	0.0008	0.0010	0.014 ns^{-1}	0.015 ns^{-1}
120	0.0003	0.0003	0.005 ns^{-1}	0.005 ns^{-1}

[a] The resonance-Coulomb and Förster rates are sums of individual rates computed for the cofacial parallel case ($\kappa_{DA}^2 = 1$).

molecule. This simplification may not be applicable for other systems; however, the generalization to include multiple donor states, as well as multiple acceptor states, is relatively straightforward.[42] The TPP acceptor molecule exhibits significant oscillator strengths from 338 nm to 429 nm (see Table 1). The aforementioned calculated excitation energies agree reasonably well with the experimental absorption spectra of PFO (385 nm) and TPP (418 nm).[52] It is expected that the effect of vibronic progression will red-shift the computed excitation energies of the PF_6 donor to wavelengths that are more representative of the vibronic bands [423 nm, (0−0); 441 nm, (0−1); 468 nm, (0−2)] in the PFO experimental spectrum. In the discussion below, we will only include EET from the lowest singlet donor excited state to acceptor states described by transition bands between 367 nm and 429 nm. Other acceptor states are not included, because their spectral overlaps with the donor band are small.

Our analysis of the couplings indicate that transition dipole moment vectors are poor depictions of transition densities at close DA separations. Table 2 displays representative values of the resonance-Coulomb coupling and the corresponding Förster approximation $[(d_A d_D/R_{DA}^3)^2]$ for several distances of the centers of mass between PF_6 and TPP. The couplings are computed from parallel orientation of transition dipole moments associated with the 358-nm donor band and the 367-nm acceptor band and orthogonal orientation of these dipole vectors relative to the DA separation (see Figure 1). Such a cofacial parallel arrangement gives an orientation factor of unity. As expected, the point-dipole approximation converges to the full coupling at large (>100 Å) interchromophore separation. The point-dipole expression, however, grossly exaggerates the coupling strength at close DA distance to give EET rates that are orders of magnitude larger than the correct value. The rates reported in Table 2 are sums of individual rates between donor chromophores characterized by the 358-nm band and acceptor chromophores characterized by the 367-, 390-, 418-, and 429-nm bands. The calculations do not take into account a distribution of orientation factors; the individual rates are all computed for the cofacial parallel case where κ_{DA}^2 is unity. A strictly parallel orientation in the Förster sense is not possible in the microscopic calculation, because the transition dipole moment changes with the electronic state. For example, a molecular arrangement of a DA pair which aligns the 358-nm donor transition dipole moment with the 367-nm acceptor transition dipole moment will no longer provide a parallel orientation when one considers the 390-nm acceptor transition. One would have to reorient the DA molecules such that the transition dipole vectors are parallel. Although the configuration-averaged square of the Förster orientation factor is $^2/_3$, a microscopic formulation of EET permits κ_{DA}^2 to vary between a value of 0 for the case of transition dipole vectors that are orthogonal both to each other and to the DA separation (cofacial orthogonal orientation) and a value of 4 for the collinear parallel/antiparallel arrangement (see Figure 1).

By constructing a natural log plot of the rate as a function of DA separation (Figure 2), we can observe the R_{DA} dependence of the excitation transfer. The resonance-Coulomb and Förster transfer rates are also computed here for the cofacial parallel alignment described previously. Panels A, B, C, and D in Figure 2 correspond to different EET processes involving donor fluorescence at 358 nm and acceptor transitions at 367, 390, 418, and 427 nm, respectively. Table 1 and Figure 2 show that there is a significant degree of EET between the donor and those acceptor states which carry very small oscillator strength. A comparison in panels B and C shows that the transitions with midrange oscillator strengths (389 and 418 nm) dominate the total rate. In fact, a separate calculation of the transfer rate between the 331-nm dark state of the donor and the 338-nm dark state of the acceptor (not shown) is on the same order of magnitude as that between bright states. Although these states do not absorb light and do not contribute to the absorption spectrum of the acceptor chromophore, they can mediate EET. This result is contrary to Förster's macroscopic formulation of EET, which relates the rate to the spectral overlap of the donor fluorescence spectrum and acceptor absorption spectrum (see eq 11). This subtle point is a manifestation of the breakdown of the point-dipole approximation. Fleming and co-workers have observed similar coupling between bright and dark states in photosynthetic antenna systems.[43]

In Figure 2, we also have shown the distance dependence predicted by the familiar Förster R_{DA}^{-6} expression (solid line). Although the Förster rate merges with the full rate at large distances (here, after ~100 Å), there are significant differences at closer DA separation. In the range 6−10 Å, the rate can be fitted empirically to R_{DA}^{-2} dependence (dashed line in Figure 2A), indicating that, at short distances, it is the local monopole nature of the transition charge density that determines the electronic coupling between the donor and the acceptor. At the shortest distance allowed by steric hindrance, the dependence of the rate is observed to be even weaker than R_{DA}^{-2}. However, this behavior is presumably unreliable, because the zero-differential overlap approximation in the PPP approach is incompatible with the orbital overlap requirement of the Dexter theory. In the regime of such small DA separations, the Dexter mechanism dominates EET and the rate is expected to decrease exponentially with increasing distance.

The resonance-Coulomb excitation transfer rates obtained at short distances are indeed quite large—of the order of 10^{12} s^{-1}—which is in agreement with the femtosecond pump−probe spectroscopic measurements of Cerullo et al., who reported a comparable high rate of EET transfer between PFO and TPP.[52] Although they analyzed their results using the Förster R_{DA}^{-6} rate expression, the present results show that the Förster rate gives the wrong distance dependence at small values of R_{DA}. If one extrapolated from the long-distance Förster regime, the Förster rate at 4 Å interchromophore separation, for example, would be exaggerated by ~3 orders of magnitude, to a femtosecond time scale, compared to the picosecond scale of the time-resolved data. From fitting the excited-state population decay of PFO using a three channel model that includes fluorescence decay described by $\tau_D = 300$ ps, exciton−exciton annihilation, and Förster-type energy transfer, Cerullo et al. obtained a value of 4.2 nm for the Förster radius.[52] This pump−probe dynamics derived value is in good agreement with the Förster radius (4.8

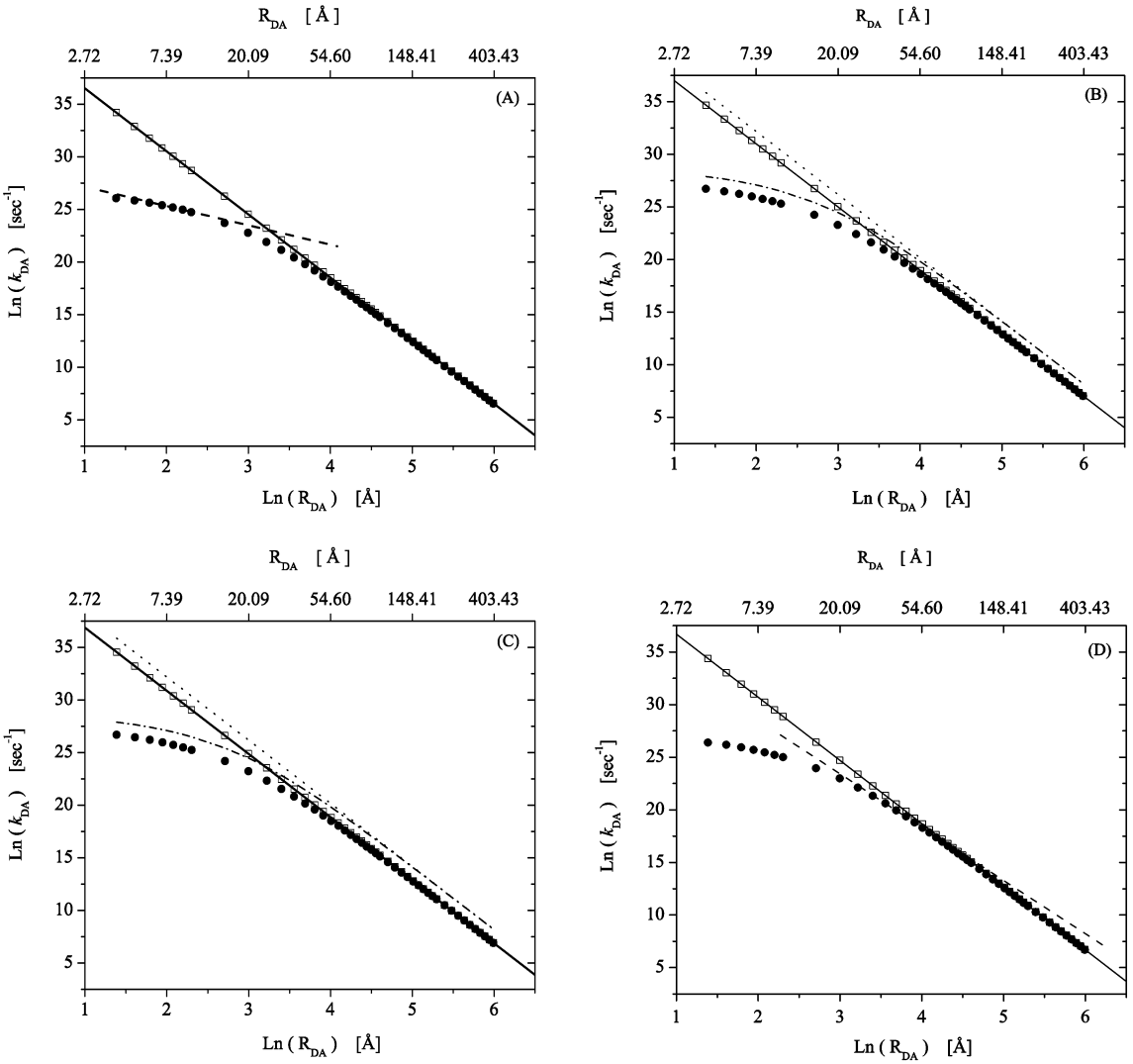

Figure 2. Distance dependence of the rate for the cofacial parallel orientation of PF_6 and TPP ((□) Förster rate and (●) resonance-Coulomb rates calculated within the PPP/SCI framework). Panels A, B, C, and D correspond to EET between the donor molecule of wavelength 358 nm to acceptor molecules of wavelengths 367, 390, 418, and 429 nm, respectively. The traditional R_{DA}^{-6} distance dependence is shown by the solid line, whereas the numerical fit of the resonance-Coulomb rates to R_{DA}^{-2} is shown by the dashed line in panel A and to R_{DA}^{-4} is shown by the dashed line in panel D. Panels B and C also provide the total Förster and resonance-Coulomb rates, summed over states, indicated by the dotted and dashed−dotted lines, respectively.

nm) computed from the overlap of the donor emission and acceptor absorption steady-state spectra but is somewhat smaller than the 5.4 nm deduced from quantum yield measurements.[80]

Our calculated value of 442 ps for the PF_6 excited state lifetime agrees reasonably with the experiment but represents a lower bound, because this rate uses eq 9 with the simplification that the product of Franck−Condon factors is unity. Defining the Förster radius as the interchromophore separation at which the probability for EET is equal to the probability for excited-state depopulation of the donor, we arrive at a value of 4.0−4.5 nm, which is consistent with the experimental analyses. If we use the resonance-Coulomb rate instead of the Förster rate, we arrive at a smaller Förster radius (3.5−4.0 nm). Although this value is not grossly different from that which is extracted based on Förster theory, it is expected that the radius obtained via these two alternative routes will deviate significantly for donors that are characterized by much shorter excited-state lifetimes. Because the experiments of Cerullo et al. were conducted in dilute concentrations of TPP in thin films of PF_6, one expects that energy transfer may involve a distribution of distances, ranging from contact to values on the order of the Förster radius R_F.

While the cofacial parallel orientation considered in the distance dependence analysis so far gives a κ_{DA}^2 value of unity, such an orientation is but one idealized choice among many possibilities within the expected distribution of orientations in condensed-phase polymeric systems. In Figure 3, we show the orientation dependence of the rate for the cofacial case, for two DA separation distances: 10 Å (Figure 3A and 3B) and 100 Å (Figure 3C and 3D). For clarity, the rates have been normalized, with respect to the maximum within each data set. Figure 3A and 3C show the orientation dependence when the transition dipole moments are aligned parallel to each other and orthogonal to the DA interchromophore axis; the angle Θ corresponds to rotation of the TPP acceptor molecule about the transition dipole moment axis (z-axis of Figure 1). Under this arrangement, the orientation factor κ_{DA}^2 is independent of rotation and is unity. Panel A shows that the rate varies by a factor of ∼2 in going from 0° to 90°, whereas the dipole approximation to the rate shows essentially negligible dependence. At large separation, as expected, rotation of TPP about the transition dipole moment axis shows weak orientation dependence of the rate (Figure 3C). Near the estimated Förster radius (not shown), the transfer rate

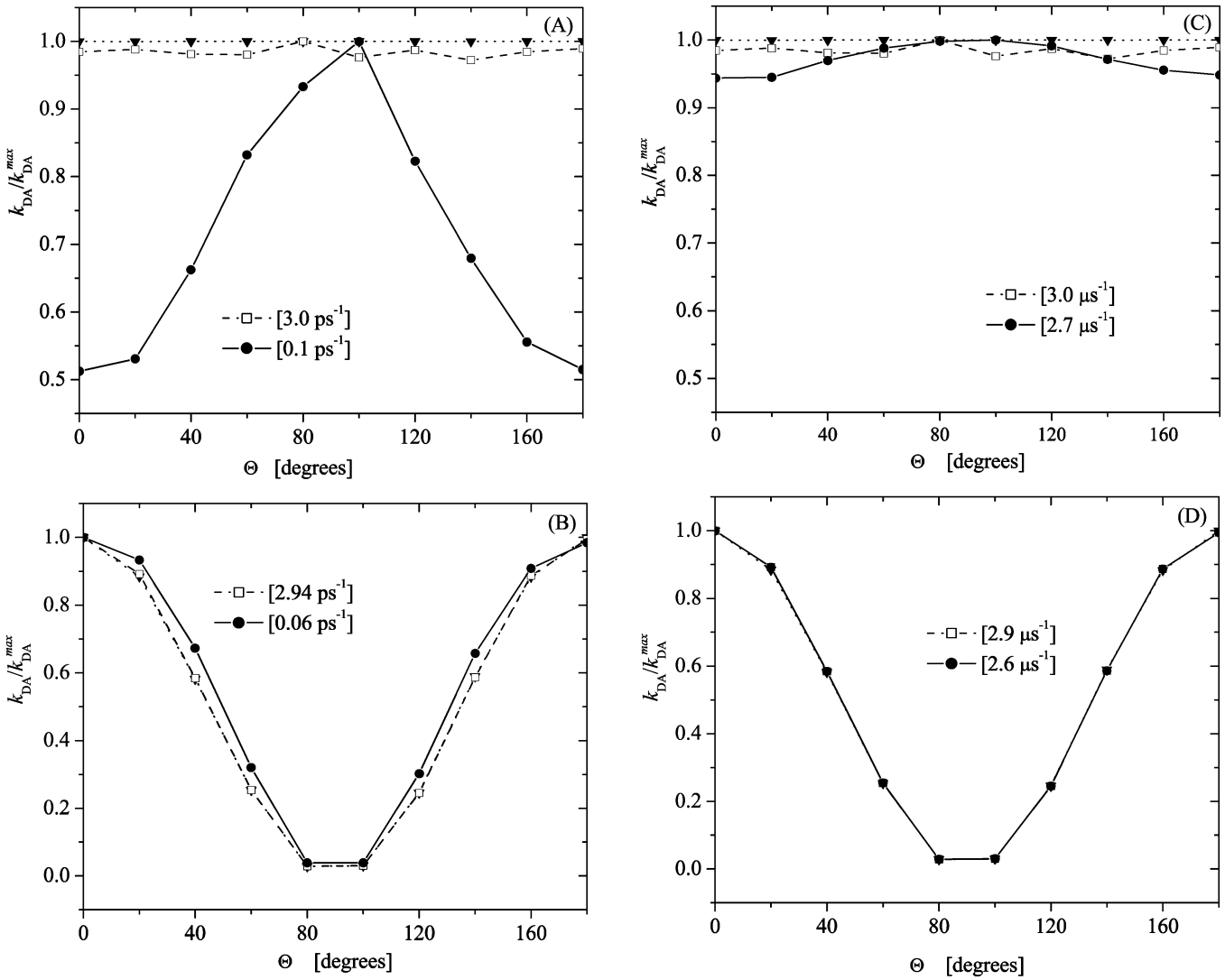

Figure 3. Orientation dependence of the normalized rate at short and long DA separation for an initial cofacial parallel alignment of the DA transition moments ((□) Förster rate, (●) resonance-Coulomb rate, and (▼) value of the orientation factor κ^2_{DA}). Panels A and C show the results of rotation of the acceptor about the transition dipole moment axis (*z*-axis) for fixed DA separations of 10 and 100 Å, respectively. Panels B and D are for rotation about an axis perpendicular to the transition moment axis (*y*-axis, Figure 1) at DA separation of 10 and 100 Å, respectively; rotation about the *x*-axis gives orientation dependence similar to that of panels B and D. The rate values given in brackets are the maximum values for that data set.

increases by ∼30% of the value for the cofacial parallel orientation. If we take the same parallel alignment of the donor and acceptor at 10 Å, but rotate TPP about either one of the axes that is perpendicular to the transition dipole moment axis, both the Förster and resonance-Coulomb couplings show the same form of systematic change as a function of angle, although the Förster expression provides couplings that are much larger. At large separations, rotation of TPP about the *x*- or *y*-axis again mirrors a cosine function of the angle between the transition dipole moment vectors (Figure 3D), and the Förster and full Coulomb rates converge.

Because even with parallel alignment of transition dipole moments at a separation of 10 Å there is a significant orientation dependence of the rate, in Figure 4, we also consider the orientation dependence for the cofacial orthogonal arrangement. The transition dipole moment vectors are aligned perpendicular to each other and perpendicular to the DA interchromophore axis and rotation is about the TPP dipole vector. Both normalized Förster and Coulomb rates show similar trends; however, the very small absolute values makes this DA orientation insignificant to EET. Even at the most optimal "orthogonal" orientation, the rate is in the time scale of hundreds per microseconds. (In principle, this molecular arrangement should provide a Θ-independent null orientation factor. As shown by the inverted solid triangle in Figure 4, the κ^2_{DA} values are indeed small but not exactly zero, because we were unable to precisely align the transition dipole vectors to be orthogonal within numerical precision.) Beljonne et al. recently reported that the resonance-Coulomb coupling can be significantly large, even for the orthogonal orientation, when the molecular center of the acceptor is displaced either longitudinally or laterally, with respect to the center of the donor.[40] We consider similar orientation and distance dependence of the transfer rate here with the molecular arrangements of the donor and acceptor depicted in Figure 5. The initial geometry corresponds to the cofacial orthogonal orientation at a DA separation of 10 Å. Translation of the TPP along the transition dipole vector of the donor is defined as the longitudinal direction, whereas translation along the transition dipole vector of the TPP acceptor is defined as the lateral direction. Whereas the orientation factor should be theoretically zero, our implementation gives values that are

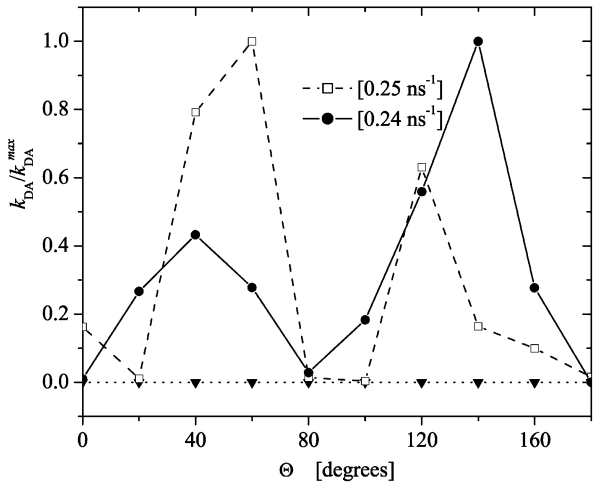

Figure 4. Orientation dependence of the normalized rate for the cofacial orthogonal arrangement of the donor and acceptor at a distance of 10 Å, where Θ denotes the angle of rotation about the acceptor TPP transition dipole moment vector (*z*-axis). Symbols denote the same quantities as in Figure 3.

small (10^{-4}) but not numerically zero, for the same reason given previously. Figure 6 shows the distance dependence of the rate for displacement along the longitudinal (panel A) and lateral (panel B) directions. The choice of negative and positive R_{DA} axes in the plots is arbitrary; however, this choice is necessary to show displacements on either side of the initial reference cofacial orthogonal configuration (defined on the plots as the points $R_{DA} = \pm 10$ Å). Moreover, the asymmetry of the plot in panel B simply reflects the asymmetry of the PF_6 transition dipole densities, with respect to the plane delineated by the position of the reference TPP molecule. For this initial DA configuration, the Förster and resonance-Coulomb rates differ by approximately an order of magnitude and are in the microsecond time scale (10 and 0.6 μs^{-1}, respectively). Although the Förster rate decreases with displacement in the longitudinal direction, the resonance-Coulomb rate increases by 3 orders of magnitude at a DA separation of ~20 Å to give excitation transfer rates in the nanosecond time scale. Displacement along the lateral direction is accompanied by approximately an order of magnitude increase in the resonance-Coulomb rate and decrease in the Förster rate. While we observe similar enhancement of the rate as reported by Beljonne et al. for the cofacial orthogonal orientation when the centers of the donor and acceptor are displaced longitudinally, we generally expect that all variants of the orthogonal orientation to all have relatively small EET rates. Excitation transfer at 1 nm in an optimal longitudinally displaced orthogonal configuration is comparable, for example, with a cofacial parallel oriented configuration with a separation of 5 nm. Because this length scale is larger than the Förster radius, it seems likely that EET would proceed via pathways that are exclusive of orthogonally oriented acceptors. Even if all the acceptors were artificially assembled in the orthogonal orientation relative to a single donor, the intrinsic radiative decay would compete efficiently. Nevertheless, the limitations of Förster theory for systems characterized by spatially delocalized transition densities and close DA separation are evident in the orientation example considered here.

The familiar R_{DA}^{-6} dependence in the Förster expression is a consequence of the decoupling of the orientation factor from the magnitudes of the transition dipole moments. Therefore, this dependence is only observed when the orientation factor is independent of the DA separation. When the orientation factor varies with DA distance, the trend can be either weaker or stronger than R_{DA}^{-6}. We encounter such a situation for the longitudinal displacement of TPP for the cofacial parallel orientation. The donor and acceptor are initially separated by 10 Å. Translation along the donor transition dipole vector is then defined as the longitudinal direction, whereas translation along the vector that is orthogonal both to the donor transition dipole moment and the DA separation vector is defined as lateral. Figure 7A shows that the orientation factor (solid inverted triangle) rapidly decreases from its initial value of 1 to 0 and then increases to an asymptotic value of 4 for longitudinal displacement; the orientation factor maintains a value of 1 for lateral displacement (panel B). Because the orientation factors are both unity for lateral translations of TPP, as well as vertical translations of TPP, along the DA intermolecular axis (see Figure 2A), it is not surprising that the Förster rates are identical in these two cases. A comparison of panels A and B of Figure 7 indicates that longitudinal displacement causes a dramatic decrease in the Förster rate—faster than the standard R_{DA}^{-6} dependence, correlated with the decrease of the orientation factor. Likewise, the resonance-Coulomb rate decreases faster for longitudinal displacements, compared to the lateral. Despite the fact that there is no simple correlation between the orientation factor and the resonance-Coulomb rate,

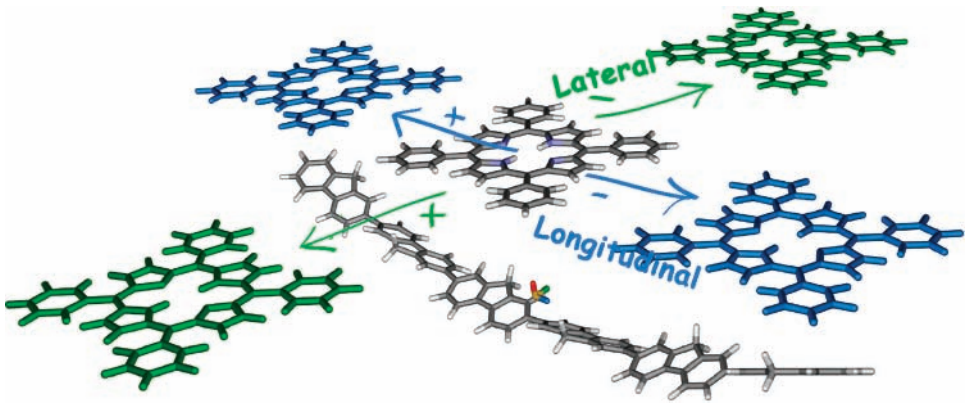

Figure 5. Geometrical arrangement of PF_6 and TPP for the study of excitation transfer rates associated with longitudinal or lateral displacement of the acceptor. The reference position of TPP corresponds to the cofacial parallel or cofacial orthogonal orientation at a DA separation of 10 Å, and the RGB-axis is identical to that in Figure 1. Displacement of TPP along the donor transition dipole moment axis (*z*-axis) is defined as the longitudinal direction, whereas displacement perpendicular to the transition dipole vector in the plane of the TPP molecule (along the *x*-axis) is defined as the lateral direction. The arbitrary choice of positive (+) and negative (−) displacement directions are also defined.

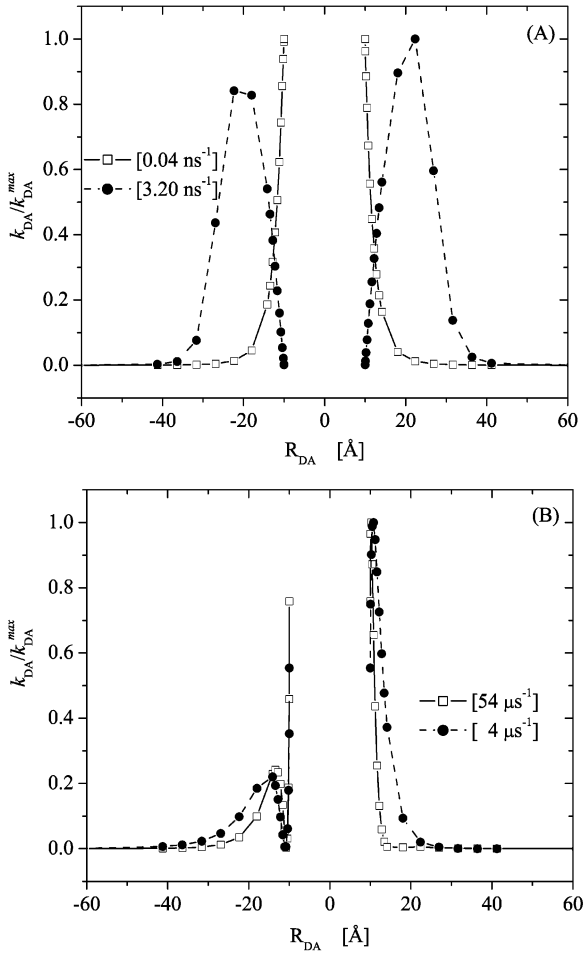

Figure 6. Distance dependence of normalized EET rates for the cofacial orthogonal orientation along the (A) longitudinal and (B) lateral directions (see Figure 5). ((□) Förster rate and (●) resonance-Coulomb rate.) Note that 10 Å corresponds to the position of closest approach for the displacement in Figure 5. The normalization factor k_{DA}^{max} is given in brackets for each data set.

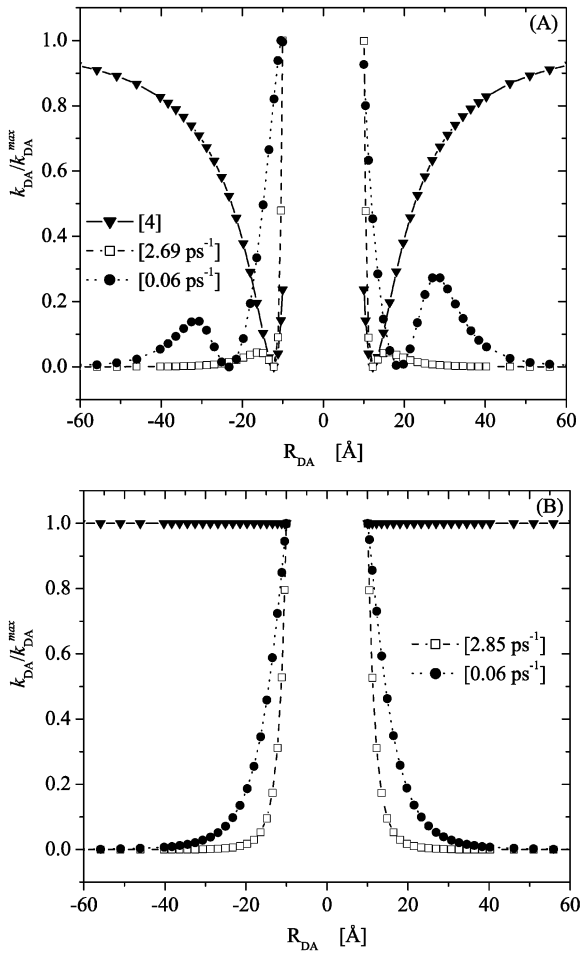

Figure 7. Distance dependence of EET rates for the cofacial parallel orientation along the (A) longitudinal and (B) lateral directions (see Figure 5). ((□) Förster rate, (●) resonance-Coulomb rate, and (▼) relative value of the orientation factor.) The value in brackets for the orientation factor is the normalization factor equal to its maximum value.

the distance dependence of the rate parallels that of the orientation factor, correlating with the dipole approximation. As κ_{DA}^2 begins to recover and monotonically increases toward the asymptotic value of 4, the Coulomb rate continues to decrease until it begins a brief recovery at a separation of ∼20 Å, only to decrease monotonically (∼30 Å) toward a rate of 0 at infinite separation. As expected, the distance dependence of the resonance-Coulomb rate at large DA separation coincides with the rates for the collinear parallel orientation where κ_{DA}^2 is 4. The complexity of the behavior is best organized by recognizing that there exists a set of curves, each individually parametrized by a single value of the orientation factor. Effectively, the plot in Figure 7A cuts across different curves associated with different orientation factors and converges to the curve where κ_{DA}^2 is at its microscopic maximum, in the collinear parallel orientation. Excitation transfer in the Förster regime, thus, is most favorable in the collinear parallel arrangement. Because the ideal cofacial parallel and collinear parallel orientations are rarely to be expected in disordered polymer systems, the orientations encountered in such systems, such as films, will be in some intermediate regime and the probability of EET will be based on a compromise between orientation and DA separation. Such an interplay between orientation and DA distance was illustrated in Figure 7A, where the orientation dependence seems to dominate at short separation (where the distance dependence is weak) and the distance dependence (which asymptotically approaches the R_{DA}^{-6} Förster character) dominates at large separation, hence, the resonance-Coulomb rate decreases, although κ_{DA}^2 monotonically increases.

5. Conclusions

Conjugated polymeric systems are characterized by polymer segments with a distribution of conjugation lengths, intersegment separations, and relative segment−segment orientations. Incoherent excitation migration among the segments is a fundamental element of the condensed-phase electronic dynamics. In relating the transfer rate to the spectral characteristics of donor emission and acceptor absorption, Förster formulated a rate expression that is amendable to direct computation, based solely on macroscopic measurements. However, the convenience and simplicity of Förster theory comes with considerable approximation. Central to the formulation is the assumption that electronic transition densities can be reduced to transition dipole moment vectors, which is an approximation that is appropriate only when the spatial scales of the densities are smaller than their separation. Furthermore, there are many known examples of efficient excitation transfer to quench sites, resulting in degraded emission quantum yield, whereas Förster theory only applies to bright states. What we have illustrated in this study is that EET, in a conjugated polymer/tetraphenylporphyrin (TPP)

donor−acceptor system, can proceed with characteristics well outside of the Förster regime for a considerable range of distances. These conclusions, in many ways, parallel the results of Fleming and co-workers in the context of photosynthesis.[43]

We have used a semiempirical quantum chemical method (PPP/SCI) to calculate the distance and orientation dependence of the electronic excitation transfer rate from a polyfluorene polymer (PF_6) segment to a TPP acceptor, which is a system that has been previously studied experimentally.[52] We found, in agreement with experiments, that the excitation energy transfer at short distances indeed occurs on the picosecond time scale. Because we can calculate the radiative rate of the donor within the same semiempirical formulation, we can also find the value of the Förster radius directly. We obtained a value of 4−4.5 nm, which is similar to the experimental results.[52] Although these experiments had been using the Förster R_{DA}^{-6} rate expression, we find that the Förster rate gives a quite inaccurate distance dependence at values of R_{DA} less than the Förster radius R_F.

Given the theoretical results obtained here, it may be worthwhile to analyze the experimental results differently. The most important result of the current calculations is the demonstration that, at short separations between the donor and the acceptor, the distance dependence is much weaker than the usual R_{DA}^{-6} value of the Förster theory. For many practical purposes, such as the fitting of the experimental results, one might use an expression of the following form:

$$k_{DA}(R) = k_D^{rad}\left(\frac{R_F}{l+R}\right)^6 \tag{17}$$

where l is an approximate measure of the conjugation length of the polymer. Clearly, such a form can reproduce the calculated distance dependence both at short and long distances.

There are several other aspects that require further attention. First, to understand the optical properties of condensed-phase conjugated polymers in general, one must characterize the rates of EET among polymer segments of varying lengths. Such work is in progress. Another general point of interest is the coupling of excitation migration to chromophore geometry and dynamics. We have considered the donor in the geometry-optimized first excited state and the acceptor in the ground state. However, when EET is rapid, then EET may occur on the same time scale as nuclear dynamics. A further complication is that, to understand fluorescence from the acceptor state, the oscillator strengths in the excited-state optimized geometry of the acceptor will be needed.

Despite these many refinements remaining, the present theoretical analysis provides considerable new insight on electronic excitation transfer in conjugated polymers and suggests several interesting routes toward further elucidation.

Appendix: Matrix Element of the Coulomb Potential between Direct Products of the Hartree−Fock and Single Excitation Determinants

We wish to evaluate the matrix element of the Coulomb potential $H' = {}^1/_2\sum_{mn} e^2/|\boldsymbol{R}_{DA} + \boldsymbol{r}_D(m) - \boldsymbol{r}_A(n)|$ between the initial state $\Psi_i = \psi_D^* \psi_A^0$ and final state $\Psi_f = \psi_D^0 \psi_A^*$:

$$\langle \Psi_i | H' | \Psi_f \rangle = \langle \psi_D^* \psi_A^0 | H' | \psi_D^0 \psi_A^* \rangle \tag{18}$$

where the superscripted asterisk and zero denote the excited and ground states, respectively, of the donor (D) and acceptor (A) molecules. Within the Hartree−Fock (HF) and single excitation configuration interaction (SCI) approach, the matrix element takes the form

$$\langle \Psi_i | H' | \Psi_f \rangle = \sum_{\substack{ar \\ \in\{D\}\in\{A\}}}^{SO} \sum_{a'r'}^{SO} C_a^r \, C_{a'}^{r'} \langle \psi_D^{a\to r} \psi_A^0 | H' | \psi_D^0 \psi_A^{a'\to r'} \rangle \tag{19}$$

where C_a^r are SCI expansion coefficients for the relevant excited state within the basis set of the determinants $\psi_D^{a\to r}$ obtained from excitation of an electron from an occupied spin−orbital (SO) a to a virtual SO r in the reference HF determinant ψ_D^0. The determinants that contribute to these matrix elements for the Coulomb potential differ by two spin−orbitals:

$$\langle \psi_D^{a\to r} \psi_A^0 | H' | \psi_D^0 \psi_A^{a'\to r'} \rangle = \langle \cdots r a' \cdots | H' | \cdots a r' \cdots \rangle \tag{20}$$

$$= \int\int d\boldsymbol{x}_1 d\boldsymbol{x}_2 \, \chi_r^*(\boldsymbol{x}_1)\chi_{a'}^*(\boldsymbol{x}_2)(e^2/r_{12}) \times (1 - \not{p}_{12})\chi_a(\boldsymbol{x}_1)\chi_{r'}(\boldsymbol{x}_2)$$

where $\not{p}_{12}$ is the permutation operator and the integration is over the spatial and spin variables ($\boldsymbol{x}_1 \equiv \{\boldsymbol{r}_1, \omega\}$) of the SO χ_r. The last equality can be found in standard quantum chemistry texts.[81] From an expansion of the molecular orbitals (MO), ψ_i, in terms of atomic orbitals $\psi_i(r) = \sum_\mu c_\mu^i \phi_\mu(r)$ and integrating over the spin variable, the matrix element in eq 20 reduces to

$$\langle \Psi_i | H' | \Psi_f \rangle = \sum_{\substack{ar \\ \in\{D\}\in\{A\}}}^{MO} \sum_{a'r'}^{MO} C_a^r \, C_{a'}^{r'} \Big[\sum_{\mu\nu\rho\sigma} c_\mu^r c_\nu^{a'} c_\rho^a c_\sigma^{r'} (2(\mu\rho|\nu\sigma) - (\mu\sigma|\nu\rho)) \Big] \tag{21}$$

where the summation is now over all occupied and virtual spatial MO (compared to summation over SO in eq 19); the factor of 2 comes from integration over the spin variable of each restricted SO within the closed-shell HF formalism. In eq 21, we use the standard notation

$$(\mu\rho|\nu\sigma) = \int\int d\boldsymbol{r}_1 d\boldsymbol{r}_2 \, \phi_\mu(1)\phi_\rho(1)(e^2/r_{12})\phi_\nu(2)\phi_\sigma(2) \tag{22}$$

Because the SCI procedure is performed within the separate donor and acceptor reference HF subspace, excitations from the donor to the acceptor, or the reverse, are not included in the summation. The last term in the aforementioned equation involves the exchange of electrons between a donor and an acceptor MO and is, therefore, neglected. In the zero-differential overlap (ZDO) approximation, $(\mu\rho|\nu\sigma) = \delta_{\mu\rho}\delta_{\nu\sigma}\gamma_{\mu\nu}$, where $\gamma_{\mu\nu} \equiv (\mu\mu|\nu\nu)$, so that the final Coulomb matrix element at the level of the PPP Hamiltonian and SCI is written as

$$\langle \Psi_i | H' | \Psi_f \rangle = \sum_{\substack{ar \\ \in\{D\}\in\{A\}}} \sum_{a'r'} C_a^r \, C_{a'}^{r'} \Big[2\sum_{\mu\nu} c_\mu^r c_\mu^a c_\nu^{a'} c_\nu^{r'} \gamma_{\mu\nu} \Big] \tag{23}$$

where $\gamma_{\mu\nu}$ represents the two-electron repulsion integral.

Acknowledgment. The authors would like to thank Dr. John Lobaugh for helpful discussions. This work was supported in part by a grant from the National Science Foundation (CHE-0134775). Additional support from the R. A. Welch Foundation is gratefully acknowledged.

References and Notes

(1) For a modern theoretical treatment of energy transfer mechanisms, see: May, V.; Kühn O. *Charge and Energy Transfer Dynamics in Molecular Systems*; Wiley-VCH: Berlin, 2000.

(2) For several recent reviews, see: Andrews, D. L., Demidov, A. A., Eds. *Resonance Energy Transfer*; Wiley: New York, 1999.
(3) van Grondelle, R.; Dekker: J. P.; Gillbro, T.; Sundström, V. *Biochim. Biophys. Acta* **1994**, *1187*, 1.
(4) Fleming, G. R.; van Grondelle, R. *Curr. Opin. Struct. Biol.* **1997**, *7*, 738.
(5) Karapetyan, N. V.; Holzwarth, A. R.; Rögner, M. *FEBS Lett.* **1999**, *460*, 395.
(6) Gobet, B.; van Grondelle, R. *Biochim. Biophys. Acta* **2001**, *1507*, 80.
(7) Melkozernov, A. N. *Photosynth. Res*. **2001**, *70*, 129.
(8) Huber, R. *Angew. Chem.* **1989**, *101*, 849.
(9) Beddard, G. S.; Porter, G.; Tredwell, C. J. *Nature* **1975**, *258*, 166.
(10) Seibert, M.; Alfano, R. R.; Shapiro, S. L. *Biochim. Biophys. Acta* **1973**, *292*, 493.
(11) Shapiro, S. L.; Kollman, V. H.; Campillo, A. J. *FEBS Lett.* **1975**, *54*, 358.
(12) Porter, G.; Tredwell, C. J.; Searle, G. F. W.; Barber, J. *Biochim. Biophys. Acta* **1978**, *501*, 232.
(13) Beddard, G. S.; Porter, G. *Nature* **1976**, *260*, 366.
(14) Byrdin, M.; Jordan, P.; Krauss, N.; Fromme, P.; Stehlik, D.; Schlodder, E. *Biophys. J*. **2002**, *83*, 433.
(15) Sener, M. K.; Lu, D.; Ritz, T.; Park, S.; Fromme, P.; Schulten, K. J. *Phys. Chem. B* **2002**, *106*, 7948.
(16) Schwartz, B. J. *Annu. Rev. Phys. Chem*. **2003**, *54*, 141.
(17) Wong, K. F.; Skaf, M. S.; Yang, C.-Y.; Rossky, P. J.; Bagchi, B.; Hu, D.; Yu, J.; Barbara, P. F. *J. Phys. Chem. B* **2001**, *105*, 6103.
(18) Hu, D.; Yu, J.; Wong, K. F.; Bagchi, B.; Rossky, P. J.; Barbara, P. F. *Nature* **2000**, *405*, 1030.
(19) Yu, J.; Hu, D.; Barbara, P. F. *Science* **2000**, *289*, 1327.
(20) Byers, J. D.; Friedrichs, M. S.; Friesner, R. A.; Webber, S. E. In *Molecular Dynamics in Restricted Geometries*; Klafter, J., Drake, J. M., Eds.; Wiley: New York, 1989; p 99.
(21) Grage, M. M.-L.; Pullerits, T.; Ruseckas, A.; Theander, M.; Inganäs, O.; Sundström, V. *Chem. Phys. Lett*. **2001**, *339*, 96.
(22) Kersting, R.; Lemmer, U.; Mahrt, R. F.; Leo, K.; Kurz, H.; Bässler, H.; Göbel, E. O. *Phys. Rev. Lett*. **1993**, *70*, 3820.
(23) Kersting, R.; Mollay, B.; Rusch, M.; Wenisch, J.; Leising, G.; Kauffmann, H. F. *J. Chem. Phys*. **1997**, *106*, 2850.
(24) Lemmer, U.; Mahrt, R. F.; Wada, Y.; Greiner, A.; Bässler, H.; Göbel, E. O. *Chem. Phys. Lett*. **1993**, *209*, 243.
(25) Hayes, G. R.; Samuel, I. D. W.; Phillips, R. T. *Phys. Rev. B* **1995**, *52*, R11569.
(26) Chen, L. H.; McBranch, D. W.; Wang, H. L.; Helgeson, R.; Wudl, F.; Whitten, D. G. *Proc. Natl. Acad. Sci. U.S.A.* **1999**, *96*, 12287.
(27) Stork, M.; Gaylord, B. S.; Heeger, A. J.; Bazan, G. C. *Adv. Mater*. **2002**, *14*, 361.
(28) Nguyen, T.-Q.; Wu, J.; Doan, V.; Schwartz, B. J.; Tolbert, S. H. *Science* **2000**, *288*, 652.
(29) Nguyen, T.-Q.; Wu, J.; Tolbert, S. H.; Schwartz, B. J. *Adv. Mater*. **2001**, *13*, 609.
(30) Schwartz, B. J.; Nguyen, T.-Q.; Wu, J.; Tolbert, S. H. *Synth. Met*. **2001**, *116*, 35.
(31) Tolbert, S. H.; Firouzi, A.; Stucky, G. D.; Chmelka, B. F. *Science* **1997**, *278*, 264.
(32) Wu, J.; Gross, A. F.; Tolbert, S. H. *J. Phys. Chem. B* **1999**, *103*, 2374.
(33) Tolbert, S. H.; Wu, J.; Gross, A. F.; Nguyen, T.-Q.; Schwartz, B. J. *Microporous Mesoporous Mater*. **2001**, *44*, 445.
(34) Yu, J.; Hu, D.; Barbara, P. F. *Science* **2000**, *298*, 1327.
(35) Hu, D.; Yu, J.; Barbara, P. F. *J. Am. Chem. Soc*. **1999**, *121*, 6936.
(36) Vanden Bout, D. A.; Yip, W.-T.; Hu, D.; Fu, D.-K.; Swager, T. M.; Barbara, P. F. *Science* **1997**, *277*, 1074.
(37) Förster, T. *Ann. Phys.* **1948**, *2*, 55.
(38) Förster, T. In *Modern Quantum Chemistry*; Sinanoglu, O., Ed.; Academic Press: New York, 1965; Vol. 3.
(39) Claudio, G. C.; Bittner, E. R. *J. Phys. Chem. A* **2003**, *107*, 7092−7100.
(40) Beljonne, D.; Pourtois, G.; Silva, C.; Hennebicq, E.; Herz, L. M.; Friend, R. H.; Scholes, G. D.; Setayesh, S.; Müllen, K.; Brédas, J.-L. *Proc. Natl. Acad. Sci. U.S.A.* **2002**, *99*, 10982.
(41) Beljonne, D.; Cornil, J.; Silbey, R.; Millié, P.; Brédas, J.-L. *J. Chem. Phys*. **2000**, *112*, 4749.
(42) (a) Scholes, G. D. *Annu. Rev. Phys. Chem.* **2003**, *54*, 57. (b) Scholes, G. D.; Jordanides, X. J.; Fleming, G. R. *J. Phys. Chem. B* **2001**, *105*, 1640.
(43) Jordanides, X. J.; Scholes, G. D.; Fleming, G. R. *J. Phys. Chem. B* **2001**, *105*, 1652.
(44) Scholes, G. D.; Fleming, G. R. *J. Phys. Chem. B* **2000**, *104*, 1854.
(45) Krueger, B. P.; Scholes, G. D.; Fleming, G. R. *J. Phys. Chem. B* **1998**, *102*, 5378.
(46) Marguet, S.; Markovitsi, D.; Millié, P.; Sigal, H. *J. Phys. Chem. B* **1998**, *102*, 4697.
(47) Markovitsi, D.; Germain, A.; Millié, P.; Lécuyer, P.; Gallos, L. K.; Argyrakis, P.; Bengs, H.; Ringsdorf, H. *J. Phys. Chem.* **1995**, *99*, 1005.
(48) Ecoffet, C.; Markovitsi, D.; Millié, P.; Lemaistre, J. P. *Chem. Phys.* **1993**, *177*, 629.
(49) Damjanović, A.; Ritz, T.; Schulten, K. *Phys. Rev. E* **1999**, *59*, 3293.
(50) Cornil, J.; Beljonne, D.; Friend, R. H.; Brédas, J. L. *Chem. Phys. Lett.* **1994**, *223*, 82.
(51) Pilcher, K.; Halliday, D. A.; Bradley, D. D. C.; Burn, P. L.; Friend, R. H.; Holmes, A. B. *J. Phys.: Condens. Matter* **1993**, *5*, 7155.
(52) Cerullo, G.; Stagira, S.; Zavelani-Rossi, M.; De Silvestri, S.; Virgili. T.; Lidzey. D. G.; Bradley, D. D. C. *Chem. Phys. Lett*. **2001**, *335*, 27.
(53) Tasch, S.; List, E. J. W.; Hochfilzer, C.; Leising, G.; Schlichting, P.; Rohr, U.; Geerts, Y.; Scherf, U.; Müllen, K. *Phys. Rev. B* **1997**, *56*, 4479.
(54) Hu, B.; Zhang, N.; Karasz, F. E. *J. Appl. Phys*. **1998**, *83*, 6002.
(55) Berggren, M.; Dodabalapur, A.; Slusher, R. E. *Appl. Phys. Lett.* **1998**, 73, 3492.
(56) Berggren, M.; Dodabalapur, A.; Slusher, R. E.; Bao, Z. *Nature* **1997**, *189*, 466.
(57) Kozlov, V. G.; Bulovic, V.; Burrows, P. E.; Forrest, R. S. *Nature* **1997**, *389*, 362.
(58) Pariser, R.; Parr, R. G. *J. Chem. Phys.* **1953**, *21*, 466.
(59) Pariser, R.; Parr, R. G. *J. Chem. Phys*. **1953**, *21*, 767.
(60) Pople, J. A. *Trans. Faraday Soc*. **1953**, *49*, 1375.
(61) Bailey, M. L. *Theor. Chim. Acta* **1969**, *13*, 56.
(62) Kuznetsov, Y. A.; Timoshenko, E. G. *J. Chem. Phys*. **1999**, *111*, 3744.
(63) Murrell, J. N.; Harget, A. J. *Semiempirical Self-Consistent-Field Molecular-Orbital Theory of Molecules*; Wiley−Interscience: London, 1972.
(64) Karabunarliev, S.; Baumgarten, M.; Müllen, K. *J. Phys. Chem. A* **2000**, *104*, 8236.
(65) Lobaugh, J.; Rossky, P. J. *J. Phys. Chem. A* **2000**, *104*, 899.
(66) Scholes, G. D.; Ghiggino, K. P. *J. Chem. Phys*. **1994**, *101*, 1251.
(67) Dexter, D. L. *J. Chem. Phys.* **1953**, *21*, 836.
(68) Harcourt, R. D.; Ghiggino, K. P. *J. Chem. Phys.* **1996**, *105*, 1897.
(69) Scholes, G. D.; Harcourt, R. D. *J. Chem. Phys*. **1996**, *104*, 5054.
(70) van der Meer, B. W. In *Resonance Energy Transfer*; Andrews, D. L.; Demidov, A. A., Eds.; Wiley: New York, 1999; pp 1−64.
(71) Haas, E.; Katchalski-Katzir, E.; Steinberg, I. Z. *Biochemistry* **1978**, *17*, 5064.
(72) Dale, R. E.; Eisinger, J.; Blumberg, W. E. *Biophys. J*. **1979**, *26*, 161.
(73) Dewar, M. J. S.; Zoebisch, E. G.; Healy, E. F.; Stewart, J. J. P. *J. Am. Chem. Soc*. **1985**, *107*, 3902.
(74) Hinze, J.; Jaffe, H. H. *J. Am. Chem. Soc.* **1962**, *84*, 540.
(75) Nishimoto, K.; Förster, L. S. *Theor. Chim. Acta* **1966**, *4*, 155.
(76) Linderberg, J. *Chem. Phys. Lett.* **1967**, *1*, 39.
(77) Garstein, Y. N.; Rice, M. J.; Conwell, E. M. *Phys. Rev. B* **1995**, *52*, 1683.
(78) Mukamel, S.; Wang, H. X. *Phys. Rev. Lett*. **1992**, *69*, 65.
(79) Mukamel, S.; Tretiak, S.; Wagersreiter, T.; Chernyak, V. *Science* **1997**, *277*, 781.
(80) Virgili, T.; Lidzey, D. G.; Bradley, D. D. C. *Adv. Mater*. **2000**, *12*, 58.
(81) See, for example: Szabo, A.; Ostlund, N. S. *Modern Quantum Chemistry: Introduction to Advanced Electronic Structure Theory*; McGraw-Hill: New York, 1989.